Estimation of Vertical Walking Ground Reaction Force in Real-life Environments using Single IMU Sensor

[Original Article]

E. Shahabpoor[1,2], A. Pavic[3]

[1]Assistant professor, Department of Architecture and Civil Engineering, University of Bath, Claverton Down, Bath, United Kingdom, BA2 7AY
[2]INSIGNEO Institute for In-silico Medicine, Department of Civil & Structural Engineering, University of Sheffield, UK
[3]Professor of Vibration Engineering, College of Engineering, Mathematics and Physical Sciences, University of Exeter, UK

Corresponding author: Erfan Shahabpoor
Department of Architecture and Civil Engineering
University of Bath
Claverton Down
Bath BA2 7AY
United Kingdom
E-mail: e.shahabpoor@bath.ac.uk
Tel: +44-012-2538-5921

Body text word count: 3424
Number of figures: 10
Number of tables: -

Abstract

Monitoring natural human gait in real-life environments is essential in many applications, including quantification of disease progression, monitoring the effects of treatment, and monitoring alteration of performance biomarkers in professional sports. Walking ground reaction forces are among the key parameters necessary for gait analysis. However, these parameters are commonly measured using force plates or instrumented treadmills which are expensive and bulky and can only be used in a controlled laboratory environment. Despite the importance of real-life gait measurement, developing reliable and practical techniques and technologies necessary for continuous real-life monitoring of gait is still an open challenge, mainly due to the lack of a practical and cost-effective wearable technology for ground reaction force measurement. This paper presents a methodology to estimate the *total* walking ground reaction force $GRF_v(t)$ in the vertical direction using data from a single inertial measurement unit. Correlation analysis of the vertical acceleration of different body segments with $GRF_v(t)$ indicated that the 7th cervical vertebrae is one of the best locations for the sensor. The proposed method improves the accuracy of the state-of-the-art $GRF_v(t)$ estimation by 25%, by utilising the time-varying ratio of the vertical acceleration of the human body centre of mass and measured C7 vertical acceleration. Results of this study showed that the proposed method estimated consistently the $GRF_v(t)$ in both indoor and urban outdoor environment, with a 4-8% peak-to-peak normalised root mean square error.

Keywords: kinetics; accelerometry;

1 Introduction

Despite the importance of long-term monitoring of walking ground reaction forces (GRFs) in medical, leisure, sports and military applications, continuous gait measurement in real-life environment is still challenging, mainly due to the lack of a practical and cost-effective wearable technology for ground reactions measurement. Several studies in the literature have proposed to estimate walking GRFs from inertial measurement (Shahabpoor and Pavic, 2017; Guo, et al., 2017; Karatsidis, et al., 2017). Recently, McDonald and Zivanovic (2013) and Bocian, et al., (2016) proposed a methodology, called 'Constant Coefficient Method' (CCM) here, in which the vertical acceleration measured at the 7th cervical vertebra ($\ddot{x}_{v,C7}(t)$) can be used to estimate the total vertical jumping and walking ground reaction forces ($GRF_v(t)$), respectively. Both studies assume that $\ddot{x}_{v,C7}(t)$ represents the movement of the body centre of mass (CoM) and, therefore, $GRF_v(t)$ can directly be estimated by multiplying the total body mass m_{total} and $\ddot{x}_{v,C7}(t)$:

$$GRF_v(t) = m_{total} \times \left(g + \ddot{x}_{v,C7}(t)\right), \quad \text{(Eq. 1)}$$

where g is the gravitational acceleration.

This study shows that this assumption might be simplistic and aims to advance the state-of-the-art in estimation of $GRF_v(t)$ from measured body acceleration by proposing an alternative methodology, termed 'Scaled Acceleration' (SA) method, to estimate $GRF_v(t)$ with higher accuracy and versatility. This research is an initial step towards developing a practical wearable sensory system to measure full body 3D kinematics and tri-axial walking ground reactions. Such system is envisaged to ultimately enable full gait analysis (including inverse dynamics) in real-life

environments with substantial application in health monitoring, diagnosis, and falls risk assessment.

Section 2.1 of the paper provides the details of the experimental campaign. The relationship between $GRF_v(t)$ and the vertical acceleration of different body segments is discussed in Section 2.2. Based on the analysis presented in Section 2.2, the 7th cervical vertebra (C7) is proposed as the optimal measurement location to estimate $GRF_v(t)$ for a single-sensor system. Section 2.3 explains in detail the proposed SA method and the results are discussed in Section 3. Finally, the conclusions are presented in Section 4 and a few suggestions are made for future research.

2 Method

2.1 Experimental procedure

Six healthy male subjects S1-S6 (age: 21 ± 1 years, weight: 77 ± 16 kg and height: 1.82 ± 0.08 m) participated in a set of walking gait measurements in the biomechanics lab at the University of Sheffield. The subjects provided informed consent in accordance with the ethical guidelines for research involving human participants at the University of Sheffield.

A bespoke grounded instrumented treadmill with two separate belts and tri-axial force measurement sensors for each foot were used to measure the tri-axial walking GRFs pertinent to each foot at 1 kHz (Bocian, et al., 2016; Racic and Brownjohn, 2011). Using the instrumented treadmill and by trial and error, the comfortable/normal walking speed of each subject was initially found to be equal to $v_{w,S1}$=1.25 m/s, $v_{w,S2}$=1.28 m/s, $v_{w,S3}$=1.28 m/s, $v_{w,S4}$=1.11 m/s, $v_{w,S5}$=1.19 m/s and $v_{w,S6}$=1.06 m/s. Then, subjects S1-S4 each participated in a set of six walking tests of 180s duration, where the treadmill speed was set to 60%, 70%, 80%, 90%, 100% and 110% of their

normal walking speed, respectively. The data of Subject S3 walking test with 110% speed was discarded due to measurement error and Subjects S5 and S6 only carried out the walking gait measurement with their normal walking speed.

In each test, the full-body 3D motion data were recorded using a CODA motion capture system (Charnwood Dynamics Limited, 2016) at 100 Hz. The marker placement protocol was based on the full-body Plug-in Gait (Vicon Motion Systems, 2016) (Figure 1).

A set of six Opal inertial measurement units (IMUs) (APDM, 2016) were used to measure the tri-axial accelerations and orientations at C7, the sternum, the 5th lumbar vertebrae (L5), the waist front (midpoint of anterior superior iliac spines) and the fourth metatarsals, with 128 Hz sampling rate (Figure 1). IMUs were placed on the body in a way that their Y axis (Z axis for fourth metatarsals) best match the vertical direction when standing straight. The tri-axial acceleration signals were then reoriented from sensors' local coordinate system to the laboratory fixed coordinate system using the orientation (quaternions) measured by the Opal IMUs with manufacturer claimed dynamic accuracy of 2.8 degrees. The range and resolution of Opal's accelerometer are ± 16g and 14 bits, respectively.

The human body was represented as an articulated multi-segment 3D system with 13 rigid segments: head, torso, pelvis, upper arms, forearms, thighs, shanks and feet. The anatomical coordinate systems and joint centre definitions used for each body segment were based on the system suggested by Ren, et al., (2008) and the segmental masses and CoM locations were determined based on Winter (1991).

All the measured data were re-sampled at 100Hz and synced in MATLAB software (Mathworks, 2016) using a trigger sync signal recorded on Opal, CODA and treadmill

systems at the beginning of each test. The raw kinematic data (tri-axial displacements) were filtered using a low pass zero lag fourth-order Butterworth digital filter with a cut-off frequency of 12 Hz to remove noise while preserving the frequency contents related to the first four harmonics of $GRF_v(t)$. The displacement signals from the motion capture system were then differentiated twice to find the corresponding acceleration signals (Zijlstra, 2004). The motion capture data were used in Section 2.2, and only the IMU-measured accelerations were used in the rest of the study for model development and validation.

From the six test participants (25 tests), 20 randomly selected tests pertinent to the subjects S1-S4 were chosen for developing the methodology, and the remaining five test data, including S5 and S6 tests, were used for validation.

For the purpose of the analysis presented in this study, the data pertinent to each complete gait cycle were extracted from the measured time histories and saved as separate data blocks. In total, 2,134 complete gait cycles were extracted from 25 tests. As the proposed SA method (Section 2.3.2) relies on identification of each gait cycle from measured $\ddot{x}_{v,C7}(t)$ signal to estimate $GRF_v(t)$, a complete gait cycle was assumed to start and finish at the $\ddot{x}_{v,C7}(t)$ single-stance local minima for a specific leg (Figure 2). This assumption was made based on our observation that the single-stance local minimum point could be identified robustly and with high accuracy from measured $\ddot{x}_{v,C7}(t)$ data for different walking regimes.

2.2 Relation between $GRF_v(t)$ and body kinematics

Based on the second Newton law and assuming that the human body is comprised of *n* solid segments, walking $GRF_v(t)$ can be estimated using:

$$GRF_v(t) = \sum_{i=1}^{n}(m_i \times (\ddot{x}_{v,i}(t) + g)), \quad \text{(Eq. 2)}$$

where, m_i is the segment 'i' mass and $\ddot{x}_{v,i}(t)$ is its CoM vertical acceleration. For each segment 'i', $\ddot{x}_{v,i}(t)$ is calculated using motion capture data and the relative location of markers on the segment with respect to the location of it's CoM.

The $GRF_v(t)$ signal estimated using measured $\ddot{x}_{v,i}(t)$ of all 13 segments (n=13) in Equation 2 is termed 'reference estimated GRF' ($GRF_{ref,estimated}(t)$) in this paper. Figure 2 compares measured $GRF_v(t)$ and corresponding $GRF_{ref,estimated}(t)$ for a typical gait cycle. The peak-to-peak normalised root mean square error (NRMSE) (Equation 3) between the $GRF_{ref,estimated}(t)$ and measured $GRF_v(t)$ was found between 2.7-6.5% with mean value of 4.4% and standard deviation of 1.1%.

$$NRMSE\ (\%) = \frac{\sqrt{\left(\sum_{t=0}^{t_{end}}\left[\left(GRF_{v,measured}(t) - GRF_{ref,estimated}(t)\right)^2\right]\right)/N}}{\max\left(GRF_{v,measured}(t)\right) - \min(GRF_{v,measured}(t))} \times 100, \quad \text{(Eq. 3)}$$

In Equation 3, t is the time vector with N samples, starting at zero and ending at t_{end}. These errors are mostly associated with assuming solid body segments, frictionless pin joints, anthropometric measurements, and skin artefacts (Winter, 1991).

For long-term continuous measurement, however, it is not practical to measure $\ddot{x}_{v,i}(t)$ of all 13 segments and the number of sensors has to be minimised. To find the best location(s) on the body for IMU sensor(s), the Pearson linear correlation of the measured $\ddot{x}_{v,i}(t)$ and corresponding $GRF_v(t)$ signals were analysed for all tests, and their average values are compared in Figure 3a. The cross-correlation coefficients were calculated for each test using Equations 4 and 5 (Fisher, 1958; Kendall, 1979) as follows:

Between $GRF_v(t)$ and segment *'i'* acceleration $\ddot{x}_{v,i}(t)$:

$$\rho\left(GRF_v(t), \ddot{x}_{v,i}(t)\right) = \frac{1}{N-1}\sum_{j=1}^{N}\left(\frac{GRF_v(t_j)-\overline{GRF_v}(t)}{\sigma_{GRF_v(t)}}\right)\left(\frac{\ddot{x}_{v,i}(t_j)-\overline{\ddot{x}_{v,i}}(t)}{\sigma_{\ddot{x}_{v,i}(t)}}\right), \qquad \text{(Eq. 4)}$$

Between segments *'i'* and *'p'* acceleration signals $\ddot{x}_{v,i}(t)$ and $\ddot{x}_{v,p}(t)$:

$$\rho\left(\ddot{x}_{v,i}(t), \ddot{x}_{v,p}(t)\right) = \frac{1}{N-1}\sum_{j=1}^{N}\left(\frac{\ddot{x}_{v,i}(t_j)-\overline{\ddot{x}_{v,i}}(t)}{\sigma_{\ddot{x}_{v,i}(t)}}\right)\left(\frac{\ddot{x}_{v,p}(t_j)-\overline{\ddot{x}_{v,p}}(t)}{\sigma_{\ddot{x}_{v,p}(t)}}\right). \qquad \text{(Eq. 5)}$$

In these equations, $\sigma_{GRF_v(t)}$, $\sigma_{\ddot{x}_{v,p}(t)}$ and $\sigma_{\ddot{x}_{v,i}(t)}$ are the standard deviation of $GRF_v(t)$, $\ddot{x}_{v,p}(t)$ and $\ddot{x}_{v,i}(t)$ signals, respectively, and $\overline{GRF_v}(t)$, $\overline{\ddot{x}_{v,p}}(t)$ and $\overline{\ddot{x}_{v,i}}(t)$ are the mean value of signals over N samples.

As can be seen in Figure 3a, the cross-correlation of $GRF_v(t)$ and $\ddot{x}_{v,i}(t)$ increases from the feet to the head. This correlation is highest at C7 and head, with the average value of 0.95. The correlation of $GRF_v(t)$ and the head vertical acceleration $\ddot{x}_{v,head}(t)$, however, was found in our measurements (by comparing the synchronised test videos and the corresponding correlation signals) to be sensitive to the intentional head movements i.e. their $\rho\left(GRF_v(t), \ddot{x}_{v,head}(t)\right)$ decreases when subjects move their head uncorrelated with their trunk.

On the other hand, the contribution of each segment to $GRF_v(t)$ during a stance cycle (using Equation 2 and averaged over all stance cycles extracted from all 20 tests) is illustrated in Figure 3b. As can be seen in this figure, the torso and then thighs have the highest contribution to $GRF_v(t)$. Theoretically, measuring directly $\ddot{x}_{v,i}(t)$ of these segments, rather than estimating them, can potentially reduce the error in the estimated $GRF_v(t)$.

Combining the conclusions from the correlation and contribution analysis above and

taking into account practicality, it can be concluded that for a single sensor system, C7 can be the optimum location for measuring $\ddot{x}_{v,C7}(t)$ to estimate $GRF_v(t)$. This is an independent observation in-line with those of McDonald and Zivanovic (2013) and Bocian, et al., (2016).

2.3 Estimation of $GRF_v(t)$ from measured $\ddot{x}_{v,C7}(t)$

Following the conclusions of Section 2.2, this Section proposes an improved methodology to estimate $GRF_v(t)$, assuming $\ddot{x}_{v,C7}(t)$ and the weight of the test subjects as known inputs.

2.3.1 Constant coefficient model

According to the second Newton law, the simplest model to estimate $GRF_v(t)$ from $\ddot{x}_{v,C7}(t)$ is a linear model in the form of:

$$GRF_v(t) = m_{total} \times (\gamma \times \ddot{x}_{v,C7}(t) + g). \quad \text{(Eq. 6)}$$

If the γ coefficient is taken as 1.0, Equation 6 represents the CCM proposed by McDonald and Zivanovic (2013) and Bocian, et al., (2016) to estimate $GRF_v(t)$ for jumping and walking, respectively. To analyse the accuracy of this model, Equation 6 with $\gamma = 1$ was used to estimate $GRF_v(t)$ for all 25 tests carried out in this study. It was found that a range of 5.0-10.5% NRMSE with mean value of 7.5% and standard deviation of 1.7% is expected in the results. Figure 4a compares a typical estimated $GRF_v(t)$ (using Equation 6) and measured $GRF_v(t)$. As it can be seen in this figure, CCM generally tends to overestimate $GRF_v(t)$ peak-to-peak values (IEEE, 2003).

Figure 4b shows the optimal γ coefficient corresponding to the subjects S1-S4 tests. For each test, γ is found so that it minimises the NRMSE error between the estimated

and measured $GRF_v(t)$ signals. As can be seen in Figure 4b, the optimal γ coefficient varies between 0.78-0.96, with no obvious dependence on the walking speed. It was further found that, similar to the walking speed, γ shows no significant correlation with the subjects' weight, height and pacing frequency. As γ varies significantly during a gait cycle (Figure 4c), estimating $GRF_v(t)$ using a constant γ coefficient such as $\gamma = 1$ in Equation 6 might be too simplistic.

2.3.2 Scaled Acceleration model

The SA method proposes to use a more realistic time-varying function $\gamma(t)$ instead of the constant γ coefficient in Equation 6 to estimate $GRF_v(t)$:

$$GRF_v(t) = m_{total} \times (\gamma(t) \times \ddot{x}_{v,C7}(t) + g). \quad \text{(Eq. 7)}$$

This is based on the observation that $\gamma(t)$ signals pertinent to different gait cycles exhibit similar patterns, as is shown in Figure 5 for tests pertinent to subjects S1-S4. This means a 'template' $\gamma_T(t)$ signal can be found for a gait cycle and used to estimate $GRF_v(t)$ from measured $\ddot{x}_{v,C7}(t)$ in Equation 7. The overarching idea is to find a *template* $\gamma_T(t)$ signal for a specific cohort of people and type of activity, and then use that template $\gamma_T(t)$ to estimate $GRF_v(t)$ from measured $\ddot{x}_{v,C7}(t)$ in Equation 7. The procedure to find $\gamma_T(t)$, as explained below, requires the direct measurement of $GRF_v(t)$. However, once the $\gamma_T(t)$ signal is calculated, the SA method can estimate $GRF_v(t)$ (for that cohort/activity/gait pathology) only using the measured $\ddot{x}_{v,C7}(t)$.

The following process was carried on tests pertinent to subjects S1-S4 to calculate $\gamma_T(t)$:

I. For each test, $\ddot{x}_{v,C7}(t)$ was calculated using the tri-axial acceleration and

orientation signals measured by the IMU at C7 and the gravitational constant g was removed from $\ddot{x}_{v,C7}(t)$.

II. The start and end point of each gait cycle was identified by finding single-stance local minima in $\ddot{x}_{v,C7}(t)$ signals for a specific leg (every other single-stance local minima in $\ddot{x}_{v,C7}(t)$).

III. For each gait cycle, $\gamma(t)$ was calculated using Equation 8:

$$\gamma(t) = (GRF_v(t) - m_{total} \times g)/(m_{total} \times \ddot{x}_{v,C7}(t)) \quad \text{(Eq. 8)}$$

IV. All $\ddot{x}_{v,C7}(t)$ and $\gamma(t)$ signals were resampled to 100 points per gait cycle (also representing the percentage of a gait cycle duration).

V. To be able to average the $\ddot{x}_{v,C7}(t)$ signals for different gait cycles, timings of all the $\ddot{x}_{v,C7}(t)$ signals were first aligned using a method called Dynamic Time Warping (DTW) (Holmes and Holmes, 2001). This is done so that the key gait events (i.e. peaks and troughs) corresponding to $\ddot{x}_{v,C7}(t)$ signals of each gait cycle happen at about the same time.

DTW warps nonlinearly two time series A(t) and B(t) (e.g. $\ddot{x}_{v,C7}(t)$ signals corresponding to two different gait cycles) in the time dimension in such a way that their peaks and troughs are aligned and their summed squared differences are minimised (Holmes and Holmes, 2001). In classic DTW process, timing of both A(t) and B(t) signals are modified to optimally match their peaks and troughs. However, for the application in this paper, the DTW process was modified in such a way that only the timing of one of the signals (e.g. A(t)) is changed during the warping process without modifying the timing of the second signal (e.g. B(t)). This allows for warping many A(t) signals (i.e. $\ddot{x}_{v,C7}(t)$ signals corresponding to different gait cycles) to a single B(t) signal (i.e. the average $\ddot{x}_{v,C7}(t)$ signal) (see

the supplementary materials for the modified DTW MATLAB code).

VI. The modified DTW procedure was used to warp all $\ddot{x}_{v,C7}(t)$ signals corresponding to different gait cycles (Figure 6a – grey curves) to the average $\ddot{x}_{v,C7}(t)$ signal (Figure 6a – dashed red curve) without modifying the timing of the average signal. This ensured that the peaks and troughs of $\ddot{x}_{v,C7}(t)$ of all gait cycles were aligned.

VII. The same warping adjustments pertinent to each $\ddot{x}_{v,C7}(t)$ signal were applied to the corresponding $\gamma(t)$ signal (Figure 6b – grey curves). This ensured that the one-to-one relationship between each pair of $\ddot{x}_{v,C7}(t)$ and $\gamma(t)$ corresponding to each gait cycle is preserved.

VIII. A pair of warped $\ddot{x}_{v,C7}(t)$ and $\gamma(t)$ signal corresponding to a gait cycle with a minimum sum of Euclidean distances to the average warped $\ddot{x}_{v,C7}(t)$ and $\gamma(t)$ signal of all the gait cycles (Figure 6a and b– dashed red curves) were chosen as the template $\ddot{x}_{T,C7}(t)$ and $\gamma_T(t)$ pair (Figure 6a and b– blue curves).

IX. A Tukey window (a rectangular window with the first and last r percent of the samples equal to parts of a cosine) with 10% tapered cosine length on each side was applied to both $\ddot{x}_{T,C7}(t)$ and $\gamma_T(t)$ signals to ensure that both curves start and finish at a same amplitude (Figure 6c and d) (see the supplementary materials for the point-by-point description of $\ddot{x}_{T,C7}(t)$ and $\gamma_T(t)$ signals). The resulting template signals can be used in a repetitive manner to estimate $GRF_v(t)$ in a gait cycle-by-cycle basis, as described in Section 2.3.2.2.

2.3.2.1 ADJUSTMENT OF $\gamma_T(t)$ AMPLITUDE FOR EACH GAIT CYCLE

To increase the accuracy of the estimated $GRF_v(t)$, it is desirable to be able to adjust both the *timing* and *amplitude* of the $\gamma_T(t)$ for each gait cycle. The timing of the $\gamma_T(t)$

283 signal is adjusted for each gait cycle using the DTW method as is explained in Section
284 2.3.2.2. The idea here is to use the (subject- and task-specific) features of measured
285 $\ddot{x}_{v,C7}(t)$ signals to find a β factor to scale the amplitude of the $\gamma_T(t)$ for each gait
286 cycle, so that the resulted gait-specific $\gamma_T(t)$ yield the best prediction of $GRF_v(t)$.

287 To adjust the $\gamma_T(t)$ amplitude, for each gait cycle, a scaling coefficient β was found
288 with trial and error, where $\beta \times \gamma_T(t)$ best matches (minimum NRMSE) the
289 corresponding $\gamma(t)$. Then, the correlation of β and $\max(\ddot{x}_{v,C7}(t))/\max(\ddot{x}_{T,C7}(t))$
290 (Figure 7a) and $\min(\ddot{x}_{v,C7}(t))/\min(\ddot{x}_{T,C7}(t))$ (Figure 7b) were analysed. It was found
291 that β and $x = \min(\ddot{x}_{v,C7}(t))/\min(\ddot{x}_{T,C7}(t))$ have the higher correlation (Figure 7).
292 Therefore, Equation 9, which describes their linear relationships, was incorporated
293 into the SA method to adjust the amplitude of the $\gamma_T(t)$ for each gait cycle:

294 $$\beta = 0.62x + 0.63 \quad \text{(Eq. 9)}$$

295 #### 2.3.2.2 $GRF_v(t)$ ESTIMATION PROCEDURE

296 The SA method proposed in this study estimates $GRF_v(t)$ using the $\ddot{x}_{v,C7}(t)$ measured
297 using a single IMU at C7 and the weight of the subject. The SA method involves the
298 following steps:

299 I. The tri-axial acceleration signals measured by the IMU at C7 in its local
300 coordinate system are re-oriented to the global/earth coordinate system using
301 the orientation of the sensor measured by the IMU (quaternions) in the global
302 coordinate system.
303 II. The measured $\ddot{x}_{v,C7}(t)$ signal is filtered using a low pass zero lag fourth-order
304 Butterworth digital filter with a cut off frequency of 12Hz, and the
305 gravitational constant g is removed.

III. The start and end point of gait cycles are identified by finding single-stance local minima for a specific leg, i.e. every other single-stance local minima in the measured $\ddot{x}_{v,C7}(t)$ signal (Figure 8a).

IV. For each gait cycle q with a period of t_q $(0 \leq t \leq t_q)$:

a. The template $\ddot{x}_{T,C7}(t)$ and $\gamma_T(t)$ signals that were calculated earlier, are resampled to match the length of the measured $\ddot{x}_{v,C7}(t)$ signal.

b. The resampled $\ddot{x}_{T,C7}(t)$ signal is warped to the measured $\ddot{x}_{v,C7}(t)$ using the modified DTW method (Figure 8b).

c. The same warping adjustments are applied to the $\gamma_T(t)$ signal to adjust its timing to the gait cycle q (Figure 8c).

d. The amplitude of the warped $\gamma_T(t)$ is then adjusted by multiplying it with the corresponding β coefficient, calculated using Equation 9 (Figure 8d).

e. The resulted $\gamma_T(t)$ signal and the measured $\ddot{x}_{v,C7}(t)$ signal are then used in Equation 10 to estimate $GRF_v(t)$ for the gait cycle q (Figure 8e):

$$GRF_v(t) = m_{total} \times \left(\gamma_T(t) \times \ddot{x}_{v,C7}(t) + g \right),\ 0 \leq t \leq t_q \qquad \text{(Eq. 10)}$$

f. Next gait cycle.

3 Results

To analyse the accuracy of the results of the SA method, Figure 9 compares the NRMSE of its estimated $GRF_v(t)$ for all 25 tests with those of the $GRF_{ref,estimated}(t)$ (Section 2.2) and CCM (McDonald and Zivanovic, 2013; Bocian, et al., 2016) with $\gamma = 1$ (Section 2.3.1). The SA method estimated $GRF_v(t)$ signals with 3.5-8.8%

NRMSE with mean value of 5.6% and standard deviation of 1.5%. As can be seen in Figure 9, the SA method estimates $GRF_v(t)$ with average 25% less error (1-3% less NRMSE) than CCM. As was expected, the accuracy of the $GRF_{ref,estimated}(t)$ was better than the SA method by 2-4% for the dataset used in this study.

3.1 Comparison with synthetic walking forces

In the absence of measurement, some methods such as the method proposed by Racic and Brownjohn (2011) are proposed in the literature to synthetically approximate a *typical* walking force signal of a subject using body/gait parameters such as walking speed and weight. Such synthetic forces include no time-dependant information such as variations of walking speed, stride length, and pacing frequency over time. On the contrary, methods such as the SA method that uses real-time measurement to estimate $GRF_v(t)$, provide an unprecedented level of reliable information about the actual timing of the gait events and GRF amplitudes experienced by a subject at each moment in time. This is particularly important in real-life environments, where the $GRF_v(t)$ can be quite different from the 'typical' synthetically generated $GRF_v(t)$.

Figure 10a compares an estimated $GRF_v(t)$ signal using the SA method with the corresponding synthetic signal estimated using the Racic and Brownjohn (2011) method, for a randomly selected measured $GRF_v(t)$ signal from the tests dataset. As can be seen in Figure 10a, the accuracy and fidelity of the $GRF_v(t)$ estimated by the SA method is considerably better than the corresponding synthetic $GRF_v(t)$.

3.2 Performance of the method in real-life environment

To analyse the performance of the SA method in real-life environment, a set of tests were carried out where 10 subjects (5 males, 5 females, age: 21 ± 4 years, weight: 73 ± 17 kg and height: 1.70 ± 0.18 m) were asked to walk normally in an urban

environment around the University of Sheffield campus on pedestrian footpaths, while wearing a pair of Tekscan F-Scan in-shoe pressure insoles (Tekscan, 2016) and an Opal IMU at C7. The walking pathway was characterised with flat parts as well as mild up-hills and down-hills. The IMU's tri-axial acceleration signals were reoriented from the sensor's local coordinate system to the laboratory fixed coordinate system using the orientation (quaternions) measured by the sensor. All the measured data were re-sampled at 100Hz and synced in MATLAB software (Mathworks, 2016) using a trigger sync signal recorded on Opal and Tekscan systems at the beginning of each test.

The pressures measured under both feet were used to calculate $GRF_v(t)$. The pressure data were calibrated using the instrumented treadmill GRFs before and after each trial to minimise the time-varying calibration errors. The calibration analysis showed that, even with calibration both at the beginning and end of each test, an NRMSE of 2-5% is inevitable in the measured $GRF_v(t)$ signals using pressure sensors data.

Figure 10b shows a typical performance of the SA method in estimating $GRF_v(t)$ in an outdoor environment. The NRMSEs of the estimated $GRF_v(t)$ in these outdoor tests were found to be between 7-11%. Considering the NRMSE of 2-5% due to pressure insoles data (compared with the instrumented treadmill data), it was concluded that the performance of the SA method in the outdoor and laboratory environment was similar.

4 Conclusions

The SA method is proposed to estimate $GRF_v(t)$ of a healthy subject using the vertical acceleration measured at C7. The SA method improves the accuracy of state-of-the-art $GRF_v(t)$ estimation using single IMU sensor by 25%, by utilising the time-varying ratio of the vertical accelerations of the human body CoM and C7. The

estimated $GRF_v(t)$ contains significant information about the gait timing and the actual loads experienced by the human body in a real-life environment. Such detailed information is otherwise absent, and currently impossible to predict using synthetic walking force models. Further research is needed to improve the accuracy, versatility and robustness of these data-driven models.

The key limitations of this study are:

1) The model development and experimental verification were carried out only on healthy subjects and for walking activity. Further investigation is needed on larger datasets from different cohorts of subjects, activities and gait pathologies to find if the proposed methodology can be generalised to other cohorts and activities, and to identify the necessary adjustments to the proposed model;

2) The model verification in an outdoor environment was carried out in an urban setting with paved footpaths and smooth surfaces. Further investigations are needed to study the adjustments required to the model, so that $GRF_v(t)$ can be estimated for rough terrain.

5 Conflict of interest statement

None of the authors have any financial or personal relationships with other people or organization that could inappropriately influence their work.

6 Acknowledgements

The authors acknowledge the financial support provided by the UK Engineering and Physical Sciences Research Council (EPSRC) for the following research grants:

- Frontier Engineering Grant EP/K03877X/1 (Modelling complex and partially identified engineering problems: Application to the individualized multiscale simulation of the musculoskeletal system);
- Platform Grant EP/G061130/2 (Dynamic performance of large civil engineering structures: an integrated approach to management, design and assessment); and

The authors also acknowledge the invaluable help of Dr Mat Bocian for walking gait measurements in Sheffield Biomechanics lab.

Figures

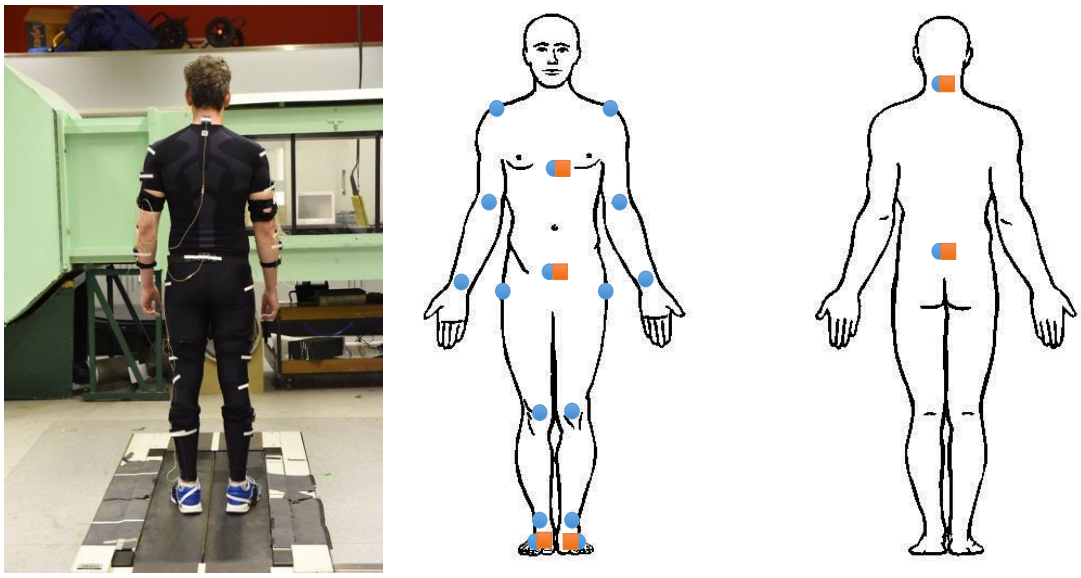

a) b)

Figure 1. (a) Subject instrumentation layout and (b) location of Coda markers (blue circles) and Opal IMUs (orange squares)

411

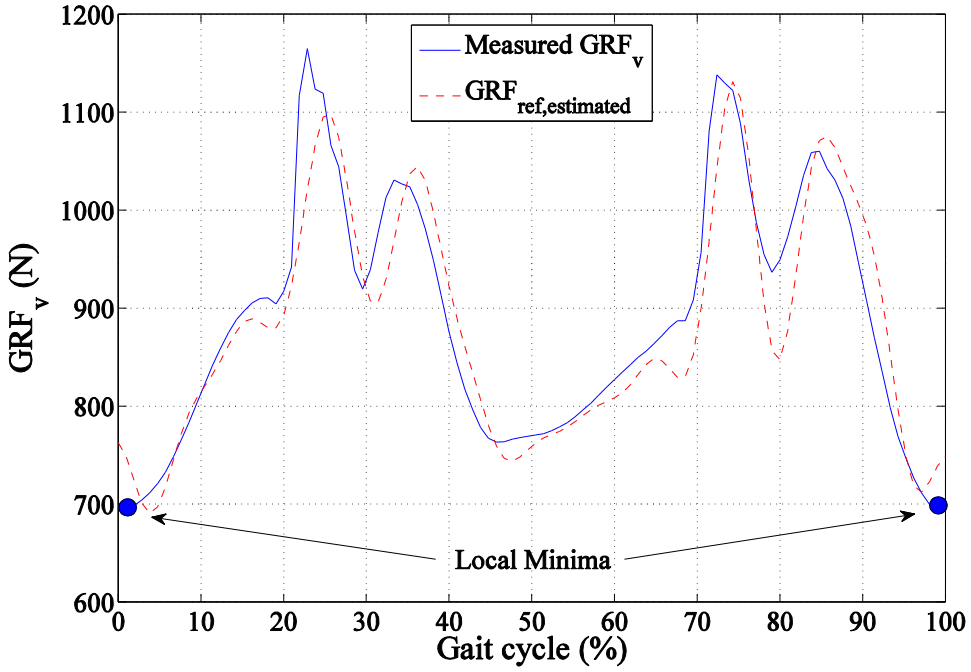

Figure 2. Comparison of the measured $GRF_v(t)$ and $GRF_{ref,estimated}(t)$ for a typical gait cycle

412

413

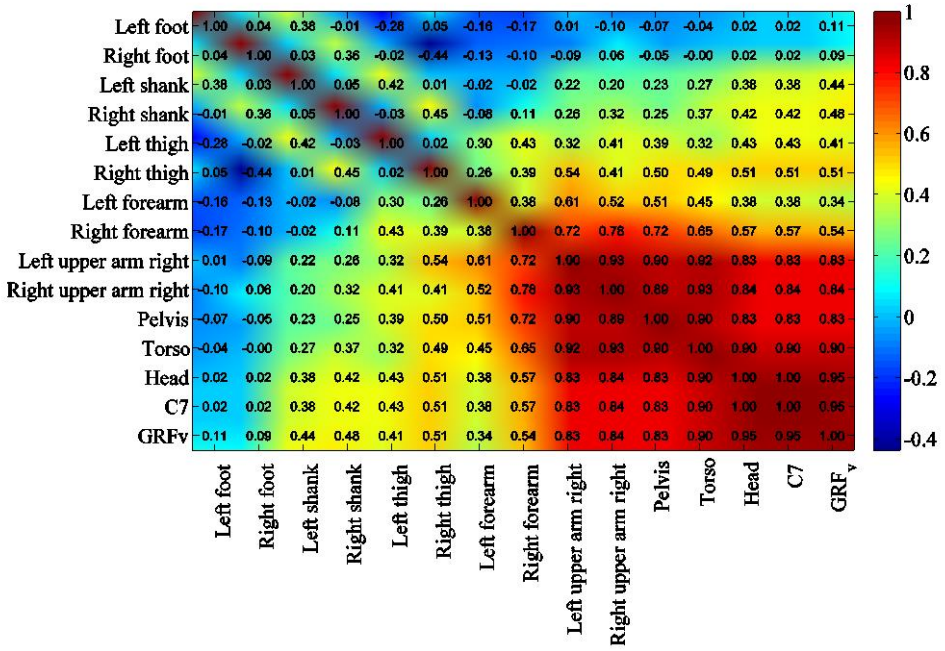

a)

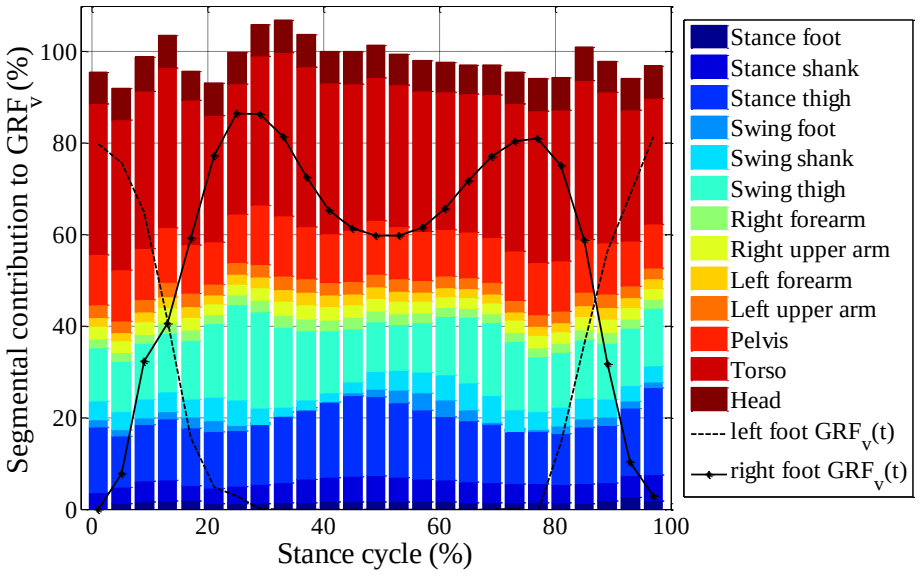

b)

Figure 3. (a) Cross correlation of $GRF_v(t)$ and the vertical segmental accelerations $\ddot{x}_{v,i}(t)$ and (b) contribution of each segment to $GRF_v(t)$.

414

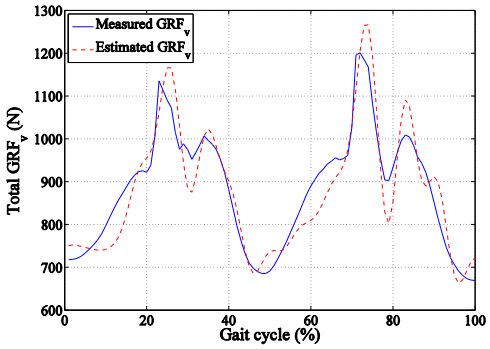

a) Comparison of the estimated and measured $GRF_v(t)$

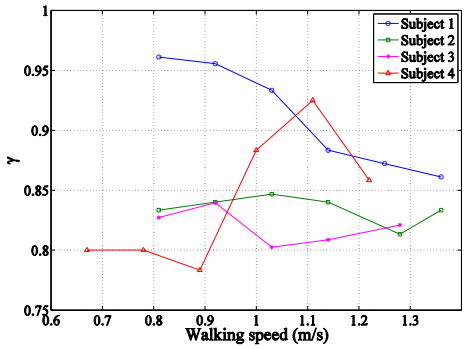

b) Optimum γ coefficient for estimated $GRF_v(t)$ in tests corresponding to the first 4 subjects

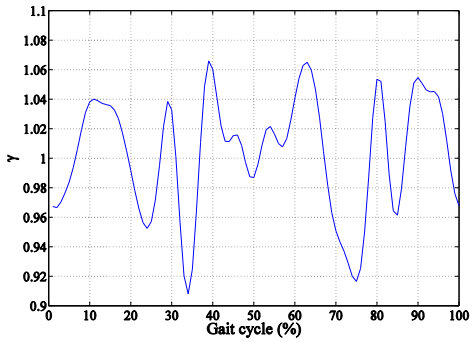

c) A typical variation of γ factor during gait cycle

Figure 4. Performance of the constant coefficient model

415

416

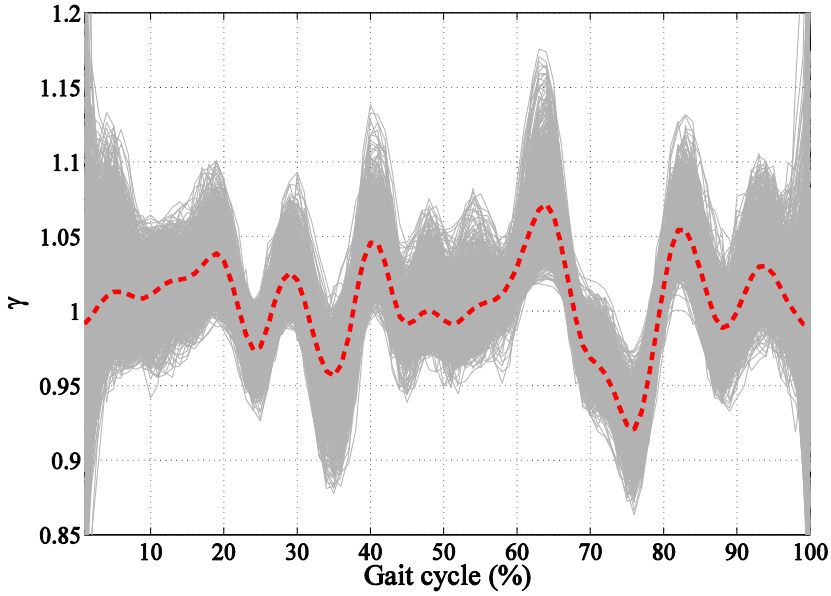

Figure 5. Variations of $\gamma(t)$ for different gait cycles for all tests pertinent to subjects S1-S4 (grey curves) and the average curve (dashed red curve)

417

418

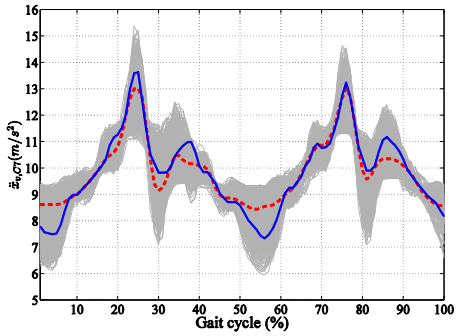

a) Variations of $\ddot{x}_{v,C7}(t)$ (including gravitation constant g) in different gait cycles (grey curves); the average curve (dashed red); and the template $\ddot{x}_{T,C7}(t)$ (solid blue curve)

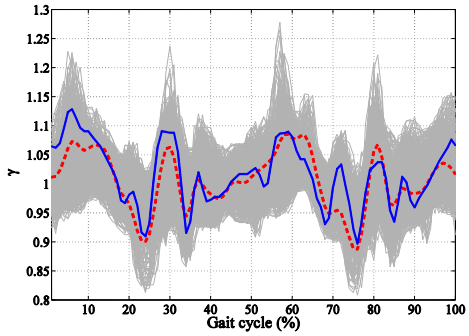

b) Variations of $\gamma(t)$ in different gait cycles (grey curves); the average curve (dashed red); and the template $\gamma_T(t)$ (solid blue curve)

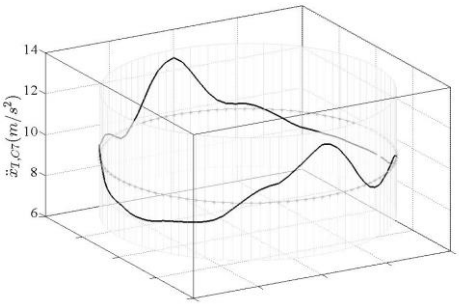

c) Cyclic illustration of $\ddot{x}_{T,C7}(t)$ (including gravitation constant g) in the polar coordinate system

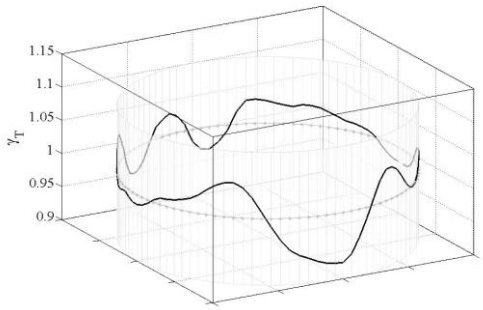

d) Cyclic illustration of $\gamma_T(t)$ in the polar coordinate system

Figure 6. The template $\ddot{x}_{T,C7}(t)$ (a and c) and $\gamma_T(t)$ (b and d) curves

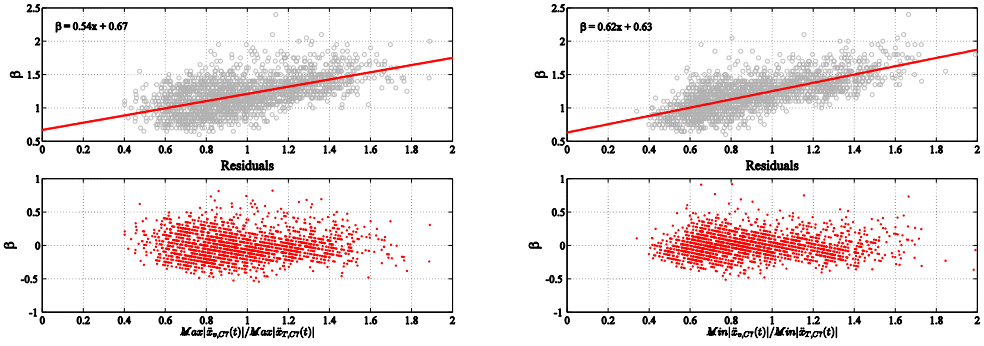

a) $\beta - \max(\ddot{x}_{v,C7}(t))/\max(\ddot{x}_{T,C7}(t))$ b) $\beta - \min(\ddot{x}_{v,C7}(t))/\min(\ddot{x}_{T,C7}(t))$

Figure 7. Defining β factor

421

422

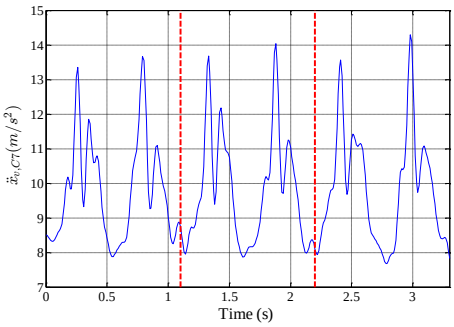

a) Identification of gait start/end points in measured $\ddot{x}_{v,C7}(t_q)$

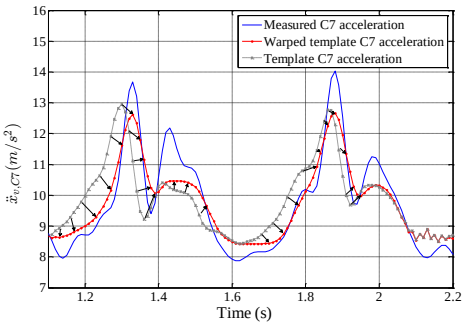

b) Warping $\ddot{x}_{T,C7}(t)$ to the measured $\ddot{x}_{v,C7}(t_q)$. Both signals include gravitation constant g for comparison.

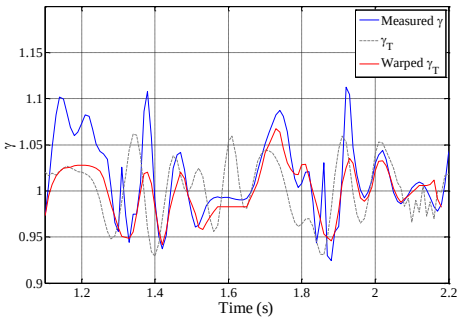

c) Applying the same warping adjustments to $\gamma_T(t)$

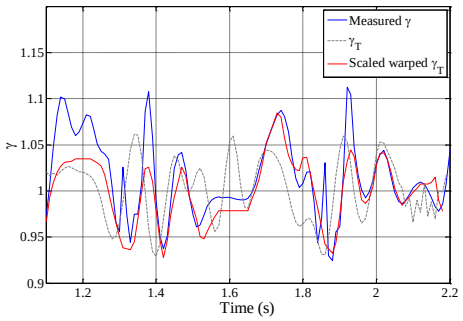

d) Scaling $\gamma_T(t)$ with β coefficient

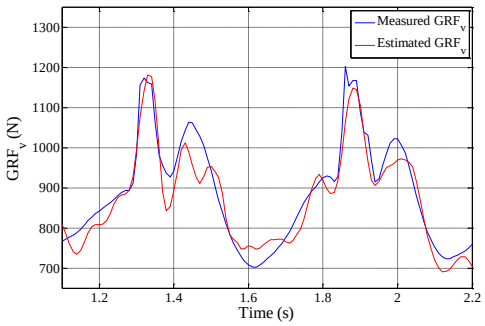

e) Estimation of $GRF_v(t)$

Figure 8. SA method procedure

423

424

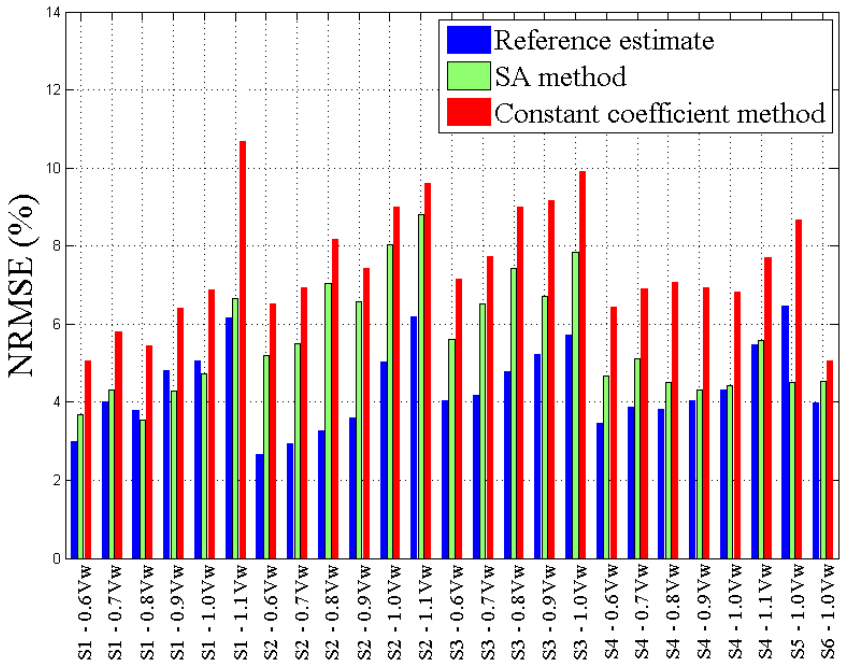

Figure 9. Comparison of the performance of the SA method with the reference estimate and CCM

425

426

427

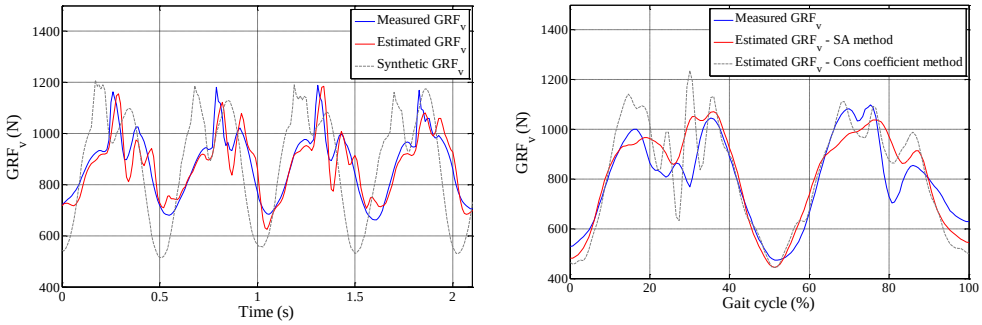

a) b)

Figure 10. Performance of the SA method in comparison with a synthetic walking force method (a) and in outdoor environment (b)

428

429

References

APDM, 2016. Mobility lab white paper. APDM website: http://www.apdm.com/wp-content/uploads/2015/10/Whitepaper1.pdf.

Bocian, M., Brownjohn, J.M.W., Racic, V., Hester, D., Quattrone, A. and Monnickendam, R., 2016. A framework for experimental determination of localized vertical pedestrian forces on full-scale structures using wireless attitude and heading reference systems. Journal of Sound and Vibration. 376, pp.217–243. http://dx.doi.org/10.1016/j.jsv.2016.05.010

Charnwood Dynamics Limited, 2016. Coda motion user's manual. Coda motion website: http://www.codamotion.com/index.php/applications/hardware/item/127-cx1-3d-scanners.

Fisher, R.A., 1958. Statistical Methods for Research Workers, 13th edition, Hafner.

Guo, Y., Storm, F., Zhao, Y., Billings, S.A., Pavic. A., Mazzà, C., and Guo, L., 2017. A New Proxy Measurement Algorithm with Application to the Estimation of Vertical Ground Reaction Forces Using Wearable Sensors. Sensors, 17, 2181; doi:10.3390/s17102181.

Holmes, J.R. and Holmes, W. 2001. Speech Synthesis and Recognition. Second edition, Taylor and Francis, London.

Institute of Electrical and Electronics Engineers, 2003. IEEE Standard on Transitions, Pulses, and Related Waveforms, IEEE Standard 181.

Karatsidis, A., Bellusci, G., Schepers, H.M., de Zee, M., Andersen, M.S., and Veltink, P.H., 2017. Estimation of Ground Reaction Forces and Moments During Gait Using

452 Only Inertial Motion Capture. Sensors 17(1), 75; doi:10.3390/s17010075.

453 Kendall, M.G., 1979. The Advanced Theory of Statistics, 4th Ed., Macmillan.

454 MathWorks, 2016. MATLAB and Statistics Toolbox Release 2016, The MathWorks,
455 Inc., Natick, Massachusetts, United States.

456 McDonald, M.G. and Zivanovic, S., 2013. Measuring Dynamic Force of a Jumping
457 Person by Monitoring Their Body Kinematics. In proceeding of 11th International
458 Conference on Recent Advances in Structural Dynamics (RASD), Italy.

459 Racic, V. and Brownjohn, J.M.W., 2011. Stochastic model of near-periodic vertical
460 loads due to humans walking. Advanced Engineering Informatics, 25, pp.259–275.
461 doi:10.1016/j.aei.2010.07.004.

462 Ren, L., Jones, R.K. and Howard, D., 2008. Whole body inverse dynamics over a
463 complete gait cycle based only on measured kinematics. Journal of Biomechanics, 41
464 pp. 2750– 2759. doi:10.1016/j.jbiomech.2008.06.001.

465 Shahabpoor, E., and Pavic, A., 2017. Measurement of Walking Ground Reactions in
466 Real-Life Environments: A Systematic Review of Techniques and Technologies.
467 Sensors, 17, 2085; doi:10.3390/s17092085.

468 Tekscan, 2016. F-Scan® In-Shoe Analysis System data sheet. Accessed online on
469 28/10/2016 at: file:///C:/Users/Erfan/Downloads/MDL-F-Scan-Datasheet%20(2).pdf.

470 Vicon Motion Systems, 2016. Bonita motion capture system data sheet. Accessed
471 online at 28/10/2016 at: https://www.vicon.com/file/vicon/bonita-brochure.pdf.

472 Winter, D.A., 1991. The biomechanics and motor control of human gait: normal,

elderly and pathological. University of Waterloo press, Ontario.

Zijlstra, W., 2004. Assessment of spatio-temporal parameters during unconstrained walking. European Journal of Applied Physiology, 92, pp.39–44, doi: 10.1007/s00421-004-1041-5.